

On the bifurcation to moving fronts in discrete systems

N. J. Balmforth^{1,2}, T. M. Janaki² and A. Kettapun³

October 6, 2004

¹*Departments of Mathematics and Earth & Ocean Science, UBC*

²*Department of Applied Mathematics and Statistics, UCSC*

³*Department of Mathematics, UCSC*

Abstract

A distinctive transition in reaction-diffusion systems is the creation of travelling fronts from stationary fronts in a pitchfork bifurcation. We explore how this bifurcation is modified when the systems are made spatially discrete. We consider two model systems: a chain of coupled Lorenz equations, and a discretized Fitz-Hugh-Nagumo model. In the former, the pitchfork bifurcation of the corresponding continuum model is replaced by a supercritical Hopf bifurcation to a pulsating front that is on average stationary, which is then followed by a heteroclinic bifurcation that glues together the pulsation cycles into an unsteadily propagating front. In the second model, the Hopf bifurcation is subcritical, the heteroclinic bifurcation glues together unstable pulsation cycles, and there is a saddle-node bifurcation in which the unstable moving front turns around into a stable one. In the vicinity of the discrete version of the bifurcation we derive an amplitude equation that qualitatively captures aspects of the two different bifurcation sequences. However, the amplitude equation is quantitatively in error apparently as a result of the beyond-all-orders nature of the effect of discreteness.

1 Introduction

Coherent structures in the form of fronts or pulses are commonly encountered solutions to reaction-diffusion systems and nonlinear field theories. This observation holds whether the system is continuous, in the sense that the field variables are defined in terms of a continuous spatial variable, or whether the system is discrete, and is arranged at the vertices of a lattice. Nevertheless, a key difference between discrete and continuous systems is that the former lack the continuous symmetry of translational invariance. As a result, it is not possible to translate a coherent structure to generate further solutions, nor for structures to propagate smoothly in space. A direct consequence is that “propagation failure” can occur in discrete systems wherein the coherent structures that propagate freely in a continuous system become “pinned” on the lattice. In nonlinear field theories like the discrete sine-Gordon equation, travelling kinks become pinned by continually shedding radiation and decelerating to rest [1, 2]. On the other hand, in some reaction-diffusion models, steady propagation can be maintained, but only provided the coupling strength between lattice sites lies above some threshold [3].

In a recent article, Pazo *et al.* [4] have presented a novel scenario describing the bifurcation to travelling kinks in a one-dimensional lattice of Lorenz systems. Kink solutions can easily be built in such systems by completely decoupling the lattice and then suitably arranging the subsystems at two different (stable) fixed points. Slowly turning the coupling back on then furnishes static kinks. As the strength of the coupling between lattice sites is further increased, Pazo *et al.* show how stationary fronts first lose stability in a Hopf bifurcation. The oscillating fronts that result remain stationary (on average) until the coupling strength is raised beyond a second threshold whereat the oscillating front collides with a second, unstable stationary kink in a heteroclinic bifurcation. This bifurcation corresponds to a gluing bifurcation of different cycles of the array. The oscillating stationary front then disappears, leaving a travelling kink.

Because the onset of kink motion is mediated by an oscillating front, Pazo & Munuzuri’s transition does not follow the usual depinning transition. In fact, it seems closely related to a different transition in reaction-diffusion systems, wherein a stationary structure loses stability in a pitchfork bifurcation and sheds a pair of propagating travelling fronts [5, 6, 7, 8]. The purpose of the present article is to establish that Pazo & Munuzuri’s transition is the discrete version of this continuum bifurcation, and to offer a compact description. We use a combination of numerical experimentation and asymptotic analysis; along the way, we expose a mathematical problem stemming apparently from the asymptotics of exponentially small terms.

2 Discrete kinks and their stability

We consider a class of coupled systems of the form,

$$\frac{d\mathbf{r}_n}{dt} = \mathbf{f}(\mathbf{r}_n) + \frac{1}{2}d\Gamma(\mathbf{r}_{n+1} + \mathbf{r}_{n-1} - 2\mathbf{r}_n), \quad (1)$$

where $\mathbf{r}_n(t)$ represents the vector of dependent variables of subsystem n , and the uncoupled ODEs have right-hand sides given by the nonlinear functions $\mathbf{f}(\mathbf{r}_n)$. The subsystems are coupled with their nearest neighbours according to a scheme given by the matrix Γ (with entries equal zero or unity), and d denotes the coupling strength. We focus on “bi-stable” subsystems which possess two stable fixed points $\mathbf{r}_n = \mathbf{R}_\pm$, plus an unstable fixed point located at the origin (so that $\mathbf{f}(\mathbf{R}_\pm) = \mathbf{f}(\mathbf{0}) = 0$). These conditions set the stage for the front dynamics, as explained further below.

The system (1) is completed with boundary conditions at the ends of the lattice. For fronts propagating on infinite lattices the natural boundary conditions are that $\mathbf{r}_n \rightarrow \mathbf{R}_\pm$ as $n \rightarrow \pm\infty$. However, for practical computations it is more convenient to study periodic lattices, with $\mathbf{r}_n \equiv \mathbf{r}_{N+n}$, for some N (a single front is then not possible, but two opposed ones work because of the reflection symmetry $n \rightarrow -n$).

Equation (1) admits stationary solutions, $\mathbf{r}_n(t) = \mathbf{R}_n$, satisfying

$$0 = \mathbf{f}(\mathbf{R}_n) + \frac{1}{2}d\Gamma(\mathbf{R}_{n+1} + \mathbf{R}_{n-1} - 2\mathbf{R}_n), \quad (2)$$

In general, we cannot solve this recursion relation explicitly, and resort to numerical techniques. However, the highly discrete, or almost uncoupled limit, is accessible to analysis: For $d = 0$, static kink solutions can be constructed by placing all subsystems to the left of a certain lattice site at \mathbf{R}_- , and all those to the right at \mathbf{R}_+ . At the distinguished lattice site, say $n = 0$, we may take either $\mathbf{R}_0 = \mathbf{R}_+$ (equivalently \mathbf{R}_- , which simply amounts to a shift of origin) or $\mathbf{R}_0 = \mathbf{0}$; both lead to kink-like solutions. By increasing d , these kink solutions can be continued to finite coupling strength. We refer to the first kind of kinks as “off-centred”, and the second type as “centred”. A key difference between the two kink solutions is that, since $\mathbf{R}_0 = \mathbf{0}$ is an unstable fixed point, we cannot expect the centred kink to be stable, whereas the off-centred kinks certainly will be at $d = 0$. To determine the stability of the kinks at arbitrary d , and in particular locate front transitions, we use the Evans function and Nyquist technology of [9].

2.1 Lorenz example

The model problem,

$$\begin{aligned} \dot{x}_n &= \sigma(y_n - x_n) \\ \dot{y}_n &= rx_n - x_n z_n - y_n + \frac{1}{2}d(y_{n+1} + y_{n-1} - 2y_n) \\ \dot{z}_n &= x_n y_n - bz_n, \end{aligned} \quad (3)$$

chains together an array of Lorenz subsystems, where r , b and σ are parameters, and was considered previously by Pazo *et al.* [10, 11, 4]. Lorenz lattices with alternative coupling schemes have also been explored [12, 13].

In figure 1, we display off-centred and centred kinks for this model with $\sigma = 10$, $b = 8/3$ and $r = 14$ (parameter values that guarantee stable fixed points at $(x, y, z) = (\pm\sqrt{b(r-1)}, \pm\sqrt{b(r-1)}, r-1)$, and

an unstable fixed point at the origin). The actual lattice computed contains sixty sites; the remainder of the infinite chain is accounted for by imposing suitable boundary conditions at the endpoints, obtained by matching the solution to an analytical one representing the “tails” of the kink. Also shown in the figure are Nyquist plots of the Evans function, $D(\lambda) = D_r(\lambda) + iD_i(\lambda)$, of each kink [9], which maps out a closed curve on the (D_r, D_i) -plane as its argument, λ (the frequency), is varied along the imaginary axis. Each encirclement of the origin by the closed contour indicates an unstable localized eigenmode. Such encirclings show that the centred kink is always unstable, and that the off-centred kink loses stability as the coupling strength is raised through a certain threshold. Moreover, the double encircling of the Nyquist plot beyond the threshold reveals a Hopf bifurcation. With further use of $D(\lambda)$, we may determine the locus of that bifurcation on the (d, σ) -plane, as shown in figure 2. The locus limits to the line $\sigma = \sigma_c = (2b + 3rb)/(2r - 5b - 2)$ as $d \rightarrow \infty$, which, as we show below, is the front bifurcation in a related continuum model.

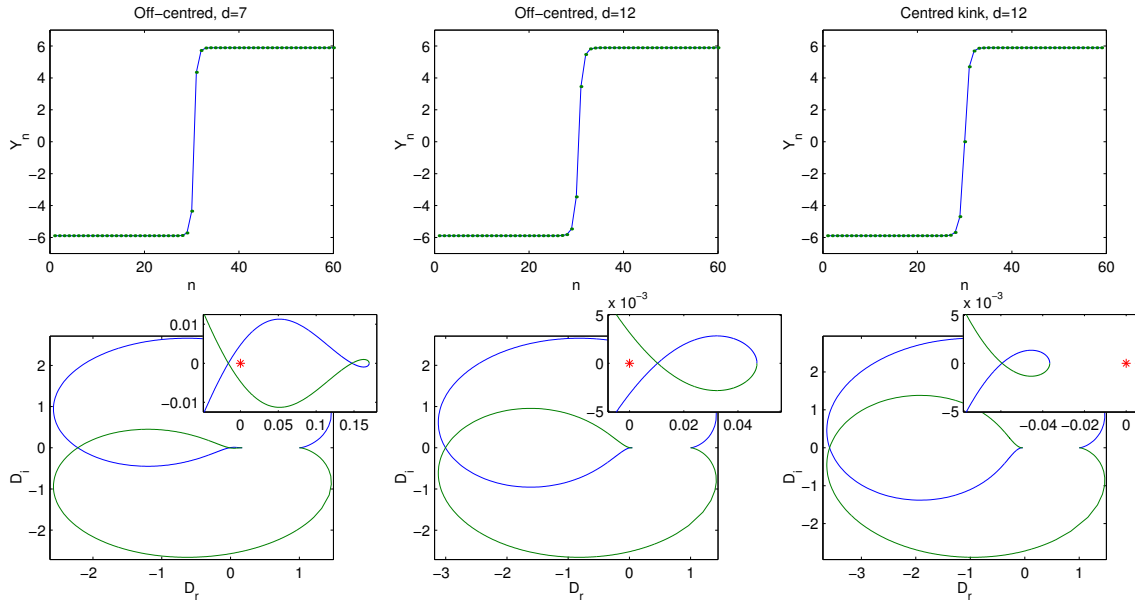


Figure 1: Fronts and Nyquist plots of the Evans function $D(\lambda)$ for three kinks of the Lorenz chain. $r = 14$, $\sigma = 10$, $b = 8/3$ and $N = 60$. As shown by the magnification of the neighbourhood of the origin, the first Nyquist plot fails to encircle the origin, whilst the second one encircles it twice; the third plot reveals a single encircling.

The dynamics close to the depinning transition is illustrated in figures 3 and 4. The first figure shows two initial-value problems just after the Hopf bifurcation that destabilizes the off-centred kink. These initial-value computations begin from states containing two opposing kinks (a kink and an “anti-kink”) so that solution satisfies periodic boundary conditions, but which are sufficiently far apart that their interaction is much weaker than the intrinsic dynamics (and instability) of each kink. Thus, the solution consists effectively of two isolated fronts, as can be verified by recomputing with a lattice of different length (N). The two computations begin near the two unstable kinks (centred and off-centred). In figure 3, both computations converge to a pulsating kink which, on average, is stationary. The top panels display the space-time evolution of the lattices on the (t, n) -plane. As shown by the panel beneath, an illuminating representation of such solutions is provided by projecting phase portraits of all the subsystems onto the $(x_n + y_n, x_n - y_n)$ -plane. Static kinks are characterized by $x_n = y_n$ and therefore appear as collections of fixed points on the $(x_n + y_n)$ -axis that accumulate in the kinks’ tails (these are the crosses and plus signs in the figure).

On raising d , the pulsating kink collides with the unstable, static, centred kink in a heteroclinic bifur-

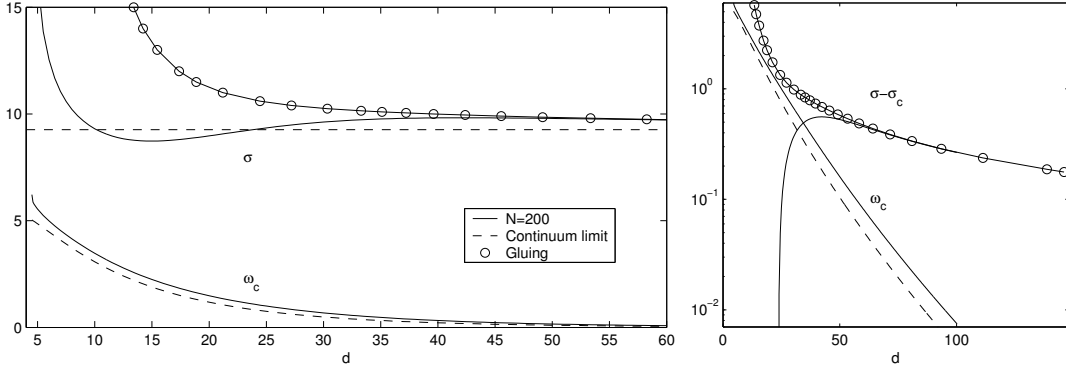


Figure 2: Locus of the Hopf and heteroclinic bifurcations on the (d, σ) -plane. Also shown is the limiting continuum bifurcation point, and the frequency, ω_c , at the Hopf bifurcation (the corresponding dashed line shows the prediction for ω_c of the asymptotic theory of section 4). The second panel shows the data on a logarithmic scale. $N = 200$, $r = 14$ and $b = 8/3$.

cation. As found by Pazo *et al.*, this is a gluing bifurcation that connects adjacent cycles of the array, and forms a travelling kink; figure 4 illustrates the dynamics beyond the heteroclinic connection. The two computations now converge to the de-pinned travelling kink. Because the moving kinks can travel in either direction, there are two possible outcomes of de-pinning: the fronts may move in the same direction, and remain isolated from one another, or they may travel toward each other and collide, in which case the system collapses to a homogeneous phase. We select initial states that avoid collisions so that we may study front evolution over a longer timescale (as in figure 4).

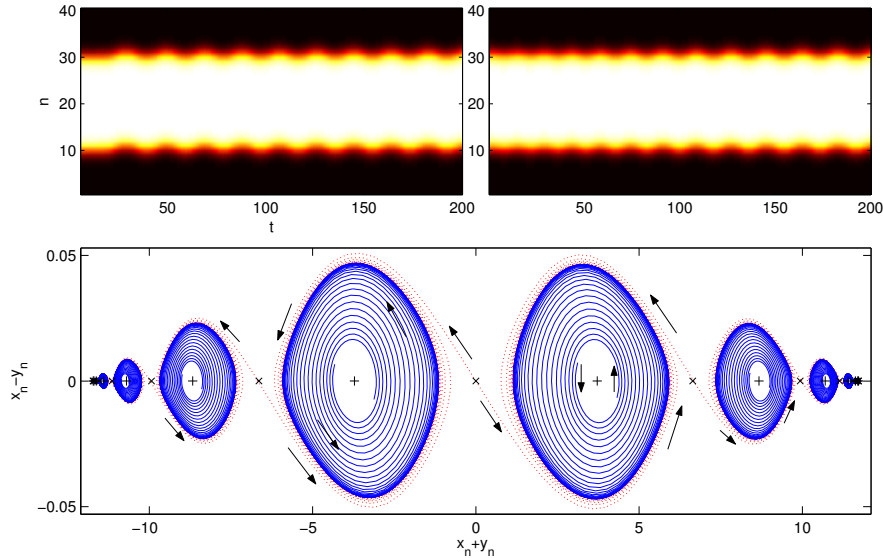


Figure 3: Fronts for $r = 14$, $\sigma = 10$, $b = 8/3$, $N = 40$ and $d = 35$. The last panel shows a phase portrait on the $(x_n + y_n, x_n - y_n)$ -plane. Evolution from near the centred and off-centred kinks are shown. The crosses and plus signs in the lower figure show the points on the two static centred and off-centred kinks.

Another useful representation of the dynamics is provided by the position and speed of each front: We estimate the instantaneous front position by linearly interpolating between the lattice points to find the

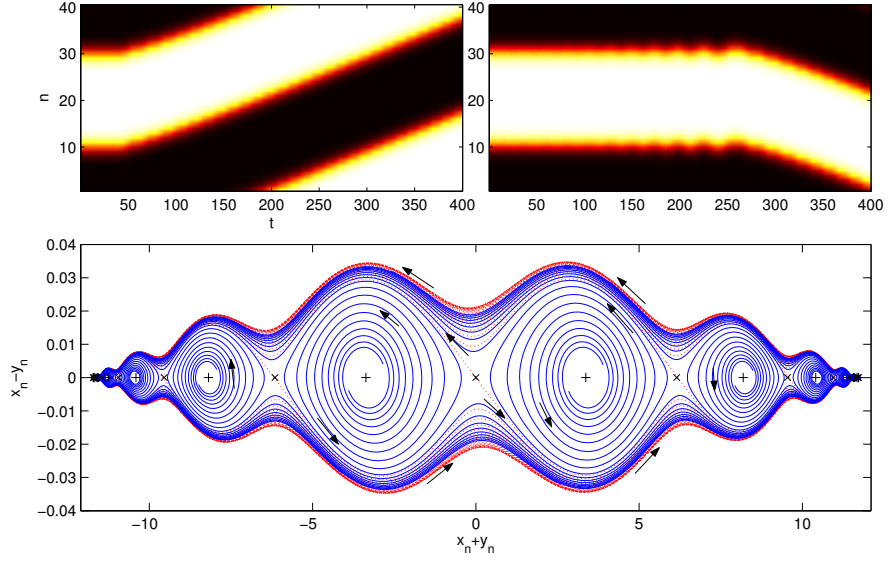


Figure 4: As in figure 3, but for $d = 42$.

location, ξ_0 , where the piecewise linear sequence of x_n 's passes through zero. Given such locations, we may numerically compute the front speed, $v = d\xi_0/dt$. Figure 5 shows the portraits of the computations in figures 3–4 on the $(\xi_0, d\xi_0/dt)$ -plane, with ξ_0 taken modulo unity.

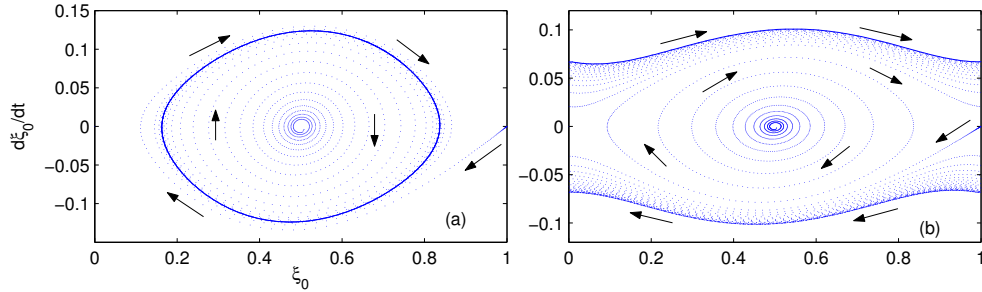


Figure 5: Phase portraits of front speeds on the $(\xi_0, d\xi_0/dt)$ -plane for the two computations shown in figures 3–4; ξ_0 is taken modulo unity. The solid lines show the stable pulsating or travelling kinks to which solutions converge.

We may also average v over a long time interval to record the mean front speed. We formulate two versions,

$$\langle d\xi_0/dt \rangle = \langle v \rangle \quad \text{and} \quad \sqrt{\langle (d\xi_0/dt)^2 \rangle} = \sqrt{\langle v^2 \rangle}, \quad (4)$$

where the angular brackets denotes the long-time average. Sample mean front speeds are presented in figure 6, and illustrate how these quantities conveniently characterize the bifurcations that set the kinks into motion: The average $\langle v \rangle$ becomes non-zero at the heteroclinic connection, whilst the root-mean-square $\sqrt{\langle v^2 \rangle}$ also records the motion of the pulsating kink. Further from the bifurcation, or nearer the continuum limit, the two averages converge to one another.

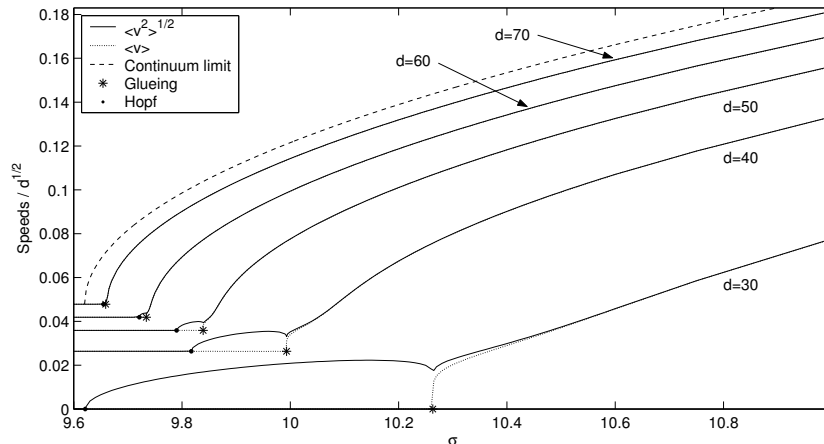


Figure 6: Front speeds for the Lorenz lattice. Shown are the average speeds defined in (4), both scaled by \sqrt{d} , against σ for five different values of d (as indicated). The stars mark the heteroclinic connection and the dots the Hopf bifurcation. The dashed line is the shape expected for the bifurcating continuum kinks close to the pitchfork. Curves are offset for clarity.

2.2 A Fitz-Hugh-Nagumo model

For a second model we consider a discretized reaction-diffusion system with the form [5],

$$\dot{x}_n = x_n - x_n^3 - y_n + \frac{1}{2}d(x_{n+1} + x_{n-1} - 2x_n), \quad \dot{y}_n = \delta(x_n - \alpha^{-1}y_n), \quad (5)$$

where δ and α are parameters. Figure 7 shows off-centred and centred kinks together with their Nyquist plots. As before, the centred kink is always unstable and the off-centred kink loses stability in a Hopf bifurcation. The locus of this bifurcation is shown on the (d, δ) -plane in figure 8.

Details of the front de-pinning process are shown in figures 9–11, which turns out to be different from the chain of Lorenz systems. In this case, the Hopf bifurcation is subcritical, and the pulsating kink solution exists at smaller d , where it is unstable. This is illustrated in figure 9, which shows front evolution close to an unstable pulsating stationary kink; one set of initial conditions spiral out to the stable moving kink, whilst the other spiral into the static off-centred kink. The solution that spirals out eventually finds a stable travelling kink, whose origin we uncover momentarily. (For the Fitz-Hugh-Nagumo model, a convenient phase portrait of the entire lattice is provided by plotting the solution on the $(x_n + y_n/\alpha, x_n - y_n/\alpha)$ -plane.)

Even though the Hopf bifurcation is subcritical, a heteroclinic connection still occurs and creates an unstable travelling front from the unstable pulsating one, albeit at smaller d . Figure 10 shows computations close to the gluing of the unstable cycles. The initial transients of these computations highlight the nearly heteroclinic orbits, and the computation spiralling out again finds a stable travelling kink.

On tracing the unstable travelling kink born in the gluing bifurcation to lower values of d , we uncover the origin of the stable travelling kink: the unstable front turns around in a saddle-node bifurcation and becomes stabilized. Figure 11 illustrates two computations with parameter settings for d that straddle the saddle-node bifurcation. One computation converges to the stable moving kink that exists at the higher value of d , whilst the other (at smaller d) hovers close by the ghost of that orbit but eventually wanders away and converges to the off-centred static kink. After its birth in the saddle-node, the stable moving front can be continued to higher coupling strengths and is, in fact, the state to which solutions converge beyond the Hopf bifurcation at higher d (figure 12).

Defining front speeds as for the Lorenz lattice (*i.e.* by linearly interpolating between the values of x_n), we may display the dynamics on the $(\xi_0, d\xi_0/dt)$ -plane. Figure 13 shows the portraits of the computations

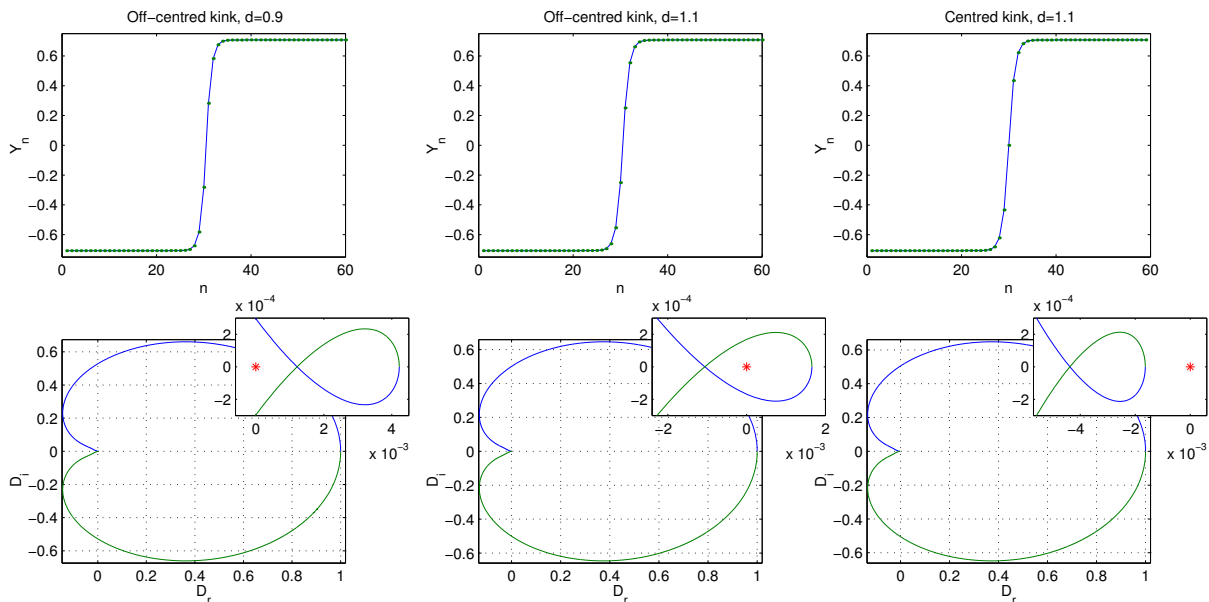


Figure 7: Fronts and Nyquist plots of the Evans function $D(\lambda)$ for three kinks of the Fitz-Hugh-Nagumo chain. $\alpha = 1/2$, $\delta = 0.24$, $\beta = 0$ and $N = 60$.

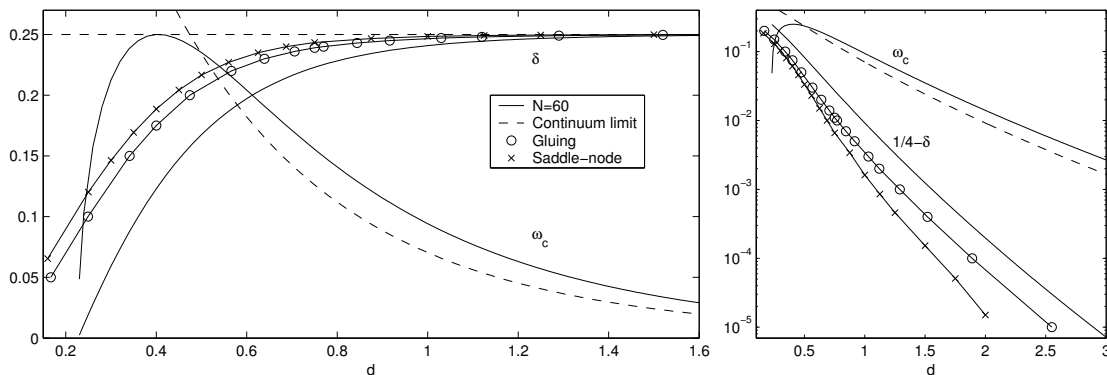


Figure 8: Locus of the Hopf, heteroclinic and saddle-node bifurcations on the (d, δ) -plane. Also shown is the limiting continuum bifurcation point, and the frequency, ω_c , at the Hopf bifurcation (the corresponding dashed line shows the prediction for ω_c of the asymptotic theory of section 4). The second panel shows the data on a logarithmic scale. $\alpha = 1/2$ and $N = 60$.

in figures 9, 10 and 12 (the portrait for figure 11 is shown in a panel of that picture). Because the Hopf bifurcation is subcritical, the pulsating kink is never observed, except possibly as an initial transient, and the average front speeds show hysteresis as one varies parameters (see figure 14).

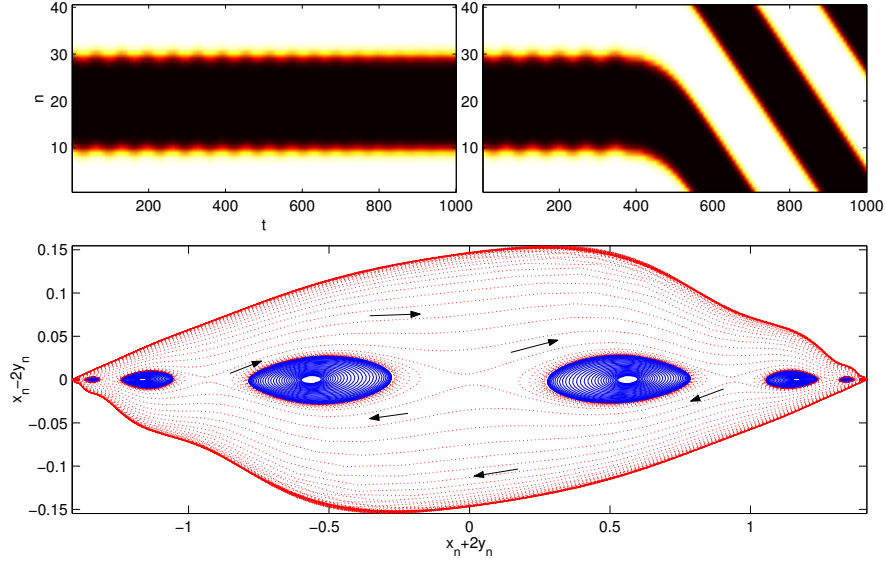


Figure 9: Evolution from near the unstable pulsating kink with initial conditions starting from inside and outside the pulsating kink: Fronts for $\alpha = 1/2$, $\delta = 0.24$, $d = 0.9$ and $N = 40$. The last panel shows a phase portrait on the $(x_n + 2y_n, x_n - 2y_n)$ -plane.

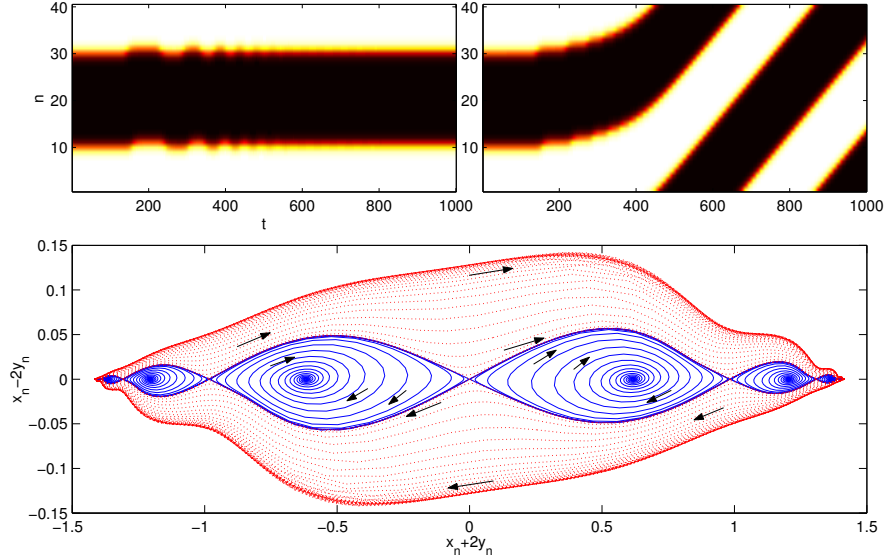


Figure 10: Evolution near the heteroclinic connection with initial conditions close to the centred kink and straddling the unstable nearly heteroclinic orbit. Fronts for $\alpha = 1/2$, $\delta = 0.24$, $N = 40$ and $d = 0.7718$.

3 Continuum model

We take the continuum limit of (1) by replacing the discrete index n with the continuous coordinate ξ , fixing $\mathbf{r}_n(t) \rightarrow \mathbf{r}(\xi, t)$, and then switching differences in n to partial derivatives in ξ :

$$\frac{\partial \mathbf{r}}{\partial t} = \mathbf{f}(\mathbf{r}) + \frac{1}{2} d \Gamma \frac{\partial^2 \mathbf{r}}{\partial \xi^2}. \quad (6)$$

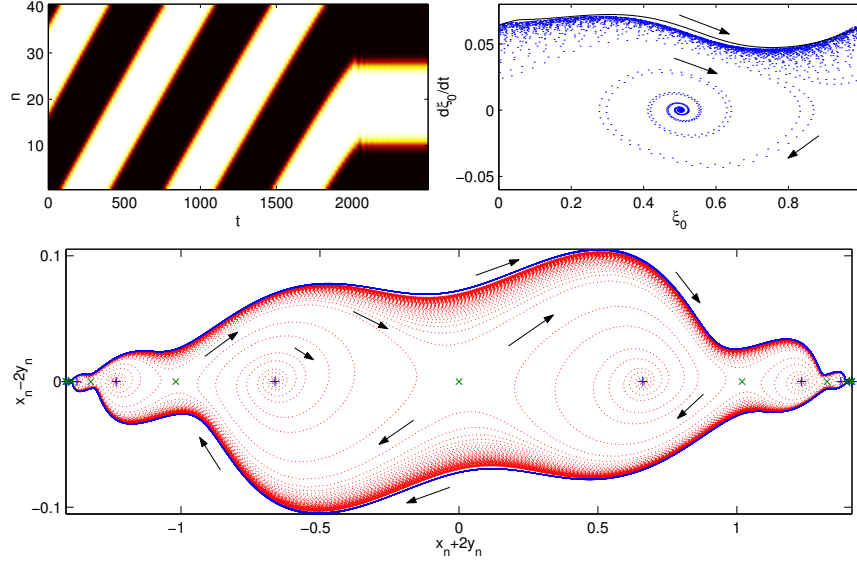


Figure 11: Evolution near the saddle-node bifurcation at $d = 0.6871$ and 0.6875 ; $\alpha = 1/2$, $\delta = 0.24$ and $N = 40$. The first panel shows the fronts for $d = 0.6871$. The second panel shows the evolution in terms of the front positions and speeds for both values of d . The solid curve shows the stable travelling kink above the saddle-node bifurcation; the evolution below that point is shown by dotted lines.

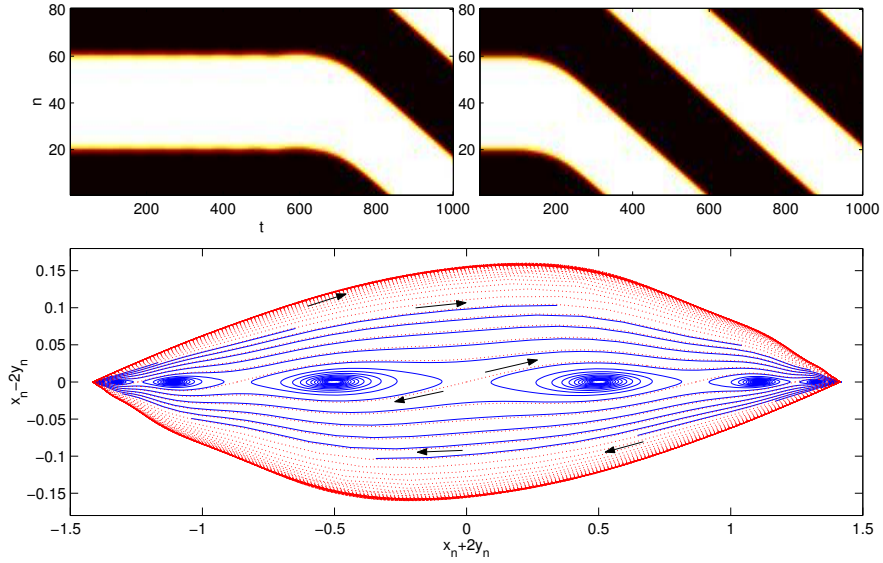


Figure 12: Evolution from near the centred and off-centred kinks for a lattice beyond the Hopf bifurcation that destabilizes the off-centred static kinks. $\alpha = 1/2$, $\delta = 0.24$, $d = 1.1$ and $N = 40$.

Note that a further scaling of ξ by \sqrt{d} can be used to eliminate that parameter from the continuum problem. This change of variable also rescales the front speed by a factor of \sqrt{d} , which has been used in displaying the data more compactly in figures 6 and 14.

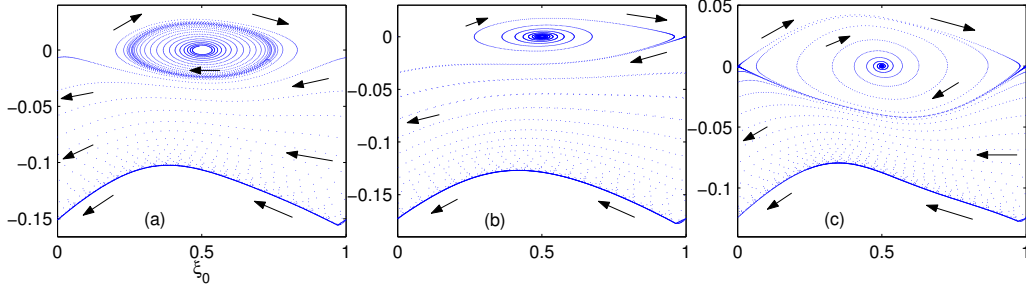


Figure 13: Phase portraits of front speeds on the $(\xi_0, d\xi_0/dt)$ -plane for the three computations shown in figures 9, 12, and 10. The solid lines show the stable travelling kinks to which solutions converge.

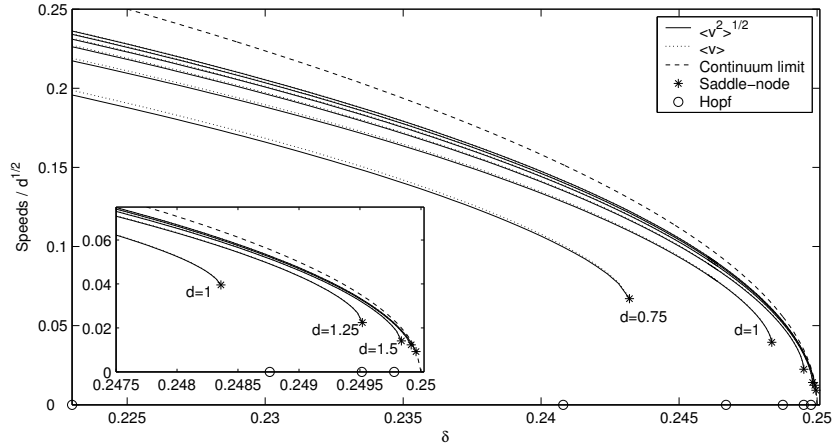


Figure 14: Front speeds for the Fitz-Hugh-Nagumo lattice. Shown are the average speeds defined in (4), both scaled by \sqrt{d} , against δ for six different values of d (0.75, 1, 1.25, 1.5, 1.75 and 2); speeds increase with d . The stars mark the saddle-node bifurcation and the circles the Hopf bifurcation. The dashed line is the shape expected for the bifurcating continuum kinks close to the pitchfork.

The continuum model has a stationary kink solution, $\mathbf{r}(\xi, t) = \mathbf{R}(\xi)$, satisfying

$$0 = \mathbf{f}(\mathbf{R}) + \frac{1}{2}d\Gamma \frac{\partial^2 \mathbf{R}}{\partial \xi^2}. \quad (7)$$

Normal-mode perturbations about this profile, with the form $\mathbf{u}(\xi)e^{\lambda t}$, satisfy the linear eigenvalue problem,

$$\lambda \mathbf{u} = J(\mathbf{R})\mathbf{u} + \frac{1}{2}d\Gamma \frac{\partial^2 \mathbf{u}}{\partial \xi^2}, \quad (8)$$

where $J(\mathbf{R})$ is the Jacobian matrix of $\mathbf{f}(\mathbf{r})$. Because of translational symmetry, (8) always has the eigen-solution, $\lambda = 0$ and $\mathbf{u} = \mathbf{R}_\xi \equiv d\mathbf{R}/d\xi$. Let \mathbf{u}^\dagger denote the adjoint to \mathbf{u} . Now, at the front bifurcation, a second eigenvalue must pass through zero, indicating that at the transition point there is a multiple, zero eigenvalue. This also demands that the eigenfunction be orthogonal to its adjoint: In terms of a standard inner product, $(\mathbf{u}^\dagger, \mathbf{u}) = 0$, which provides a simple discriminant for detecting the front bifurcation (*cf.* [14]).

3.1 Lorenz example

For the chain of Lorenz systems, the continuum model is

$$\begin{aligned} x_t &= \sigma(y - x) \\ y_t &= rx - xz - y + \frac{1}{2}dy_{\xi\xi} \\ z_t &= xy - bz. \end{aligned} \tag{9}$$

The kink is given by $x = y = Y(\xi)$ and $z = Y^2/b$, where

$$\frac{1}{2}dY_{\xi\xi} + (r - 1)Y - \frac{1}{b}Y^3 = 0, \tag{10}$$

with solution,

$$Y = \sqrt{b(r - 1)} \tanh \left[\sqrt{\frac{r - 1}{d}}(\xi - \xi_0) \right], \tag{11}$$

where ξ_0 again centres the kink.

Normal-mode solutions are given by $(\hat{x}, \hat{y}, \hat{z})e^{\lambda t}$, and satisfy linear problem,

$$\frac{1}{2}d\hat{y}_{\xi\xi} = \left[\lambda + 1 - \frac{r\sigma}{\lambda + \sigma} + \frac{(\sigma + b)\lambda + 3\sigma b}{b(\lambda + b)(\lambda + \sigma)}Y^2 \right] \hat{y}. \tag{12}$$

This equation can be solved in terms of associated Legendre functions. It can then be deduced that the front bifurcation occurs for

$$\sigma = \sigma_c = \frac{2b + 3rb}{2r - 5b - 2}. \tag{13}$$

3.2 Fitz-Hugh-Nagumo example

Hagberg & Meron [5] consider the reaction-diffusion system,

$$x_t = x - x^3 - y + \frac{1}{2}dx_{\xi\xi}, \quad y_t = \frac{\delta}{\alpha}(\alpha x - y), \tag{14}$$

which we discretized earlier. The equilibrium, steady front solution satisfies

$$0 = (1 - \alpha)x - x^3 + \frac{1}{2}dx_{\xi\xi}, \tag{15}$$

and can be taken to be

$$x(\xi) = \sqrt{1 - \alpha} \tanh \left[\sqrt{\frac{1 - \alpha}{d}}(\xi - \xi_0) \right]. \tag{16}$$

The front bifurcation occurs for $\delta = \alpha^2$. Analysis about this transition point can be used to show that the unsteady position of the moving front, $\xi_0(t)$, is given by (*cf.* [5])

$$\frac{d^2\xi_0}{dt^2} \approx -\frac{1}{\alpha}(\delta - \alpha^2)\frac{d\xi_0}{dt} - \frac{4(1 - \alpha)}{5\alpha d} \left(\frac{d\xi_0}{dt} \right)^3. \tag{17}$$

i.e. the leading-order normal form of a pitchfork bifurcation for the front speed, $v = d\xi_0/dt$.

4 Perturbation theory in the continuum limit

4.1 Derivation for the Fitz-Hugh-Nagumo example

We now present an analysis of the continuum limit that connects the continuum front bifurcation with the discrete version of the transition. We perform the analysis explicitly with the discretized Fitz-Hugh-Nagumo model, which is substantially simpler, then quote the analogous, final result for the Lorenz case.

We first rewrite the system as a PDE in terms of the continuum variables, $x(\xi, t)$ and $y(\xi, t)$:

$$\frac{1}{2}d x_{\xi\xi} + x - x^3 - y = x_t + (x_t - x + x^3 + y)\rho(\xi) \quad (18)$$

and

$$y = \alpha x - \delta^{-1}\alpha y_t = \alpha x - \frac{\alpha^2}{\delta}x_t + \frac{\alpha^3}{\delta^2}x_{tt} - \frac{\alpha^4}{\delta^3}x_{ttt} + \dots, \quad (19)$$

where

$$\rho(\xi) = \sum_{n=-\infty}^{\infty} \delta(n - \xi) - 1 \equiv 2 \sum_{k=1}^{\infty} \cos 2\pi k\xi \quad (20)$$

(*cf.* [15, 16]). Equation (18) is easily verified on finding the linear-in- ξ solution for $x(\xi, t)$ between lattice points, and then integrating the delta functions across each such point, bearing in mind that those functions create jumps in the spatial derivative of $x(\xi, t)$. We have also “iterated” (19) in preparation for the coming theory. A key point is that, as we approach the continuum limit, and close to the bifurcation that sets the kinks into motion, the term involving $\rho(\xi)$ on right-hand side of (18) is in some sense small, and the system reduces to the continuum PDEs. For now, we simply assert that this is the case and indicate later how this could be so, although there are some murky details hidden in the analysis that we expose in section 4.3.

We proceed by adopting a small parameter ε that organizes an asymptotic expansion suitable for the continuum limit. We delay the exact definition of this parameter until later because, although d^{-1} is small in the continuum limit, it is not the relevant small parameter. With ε , we quantify a distinguished limit of the problem: First, if we look close to the onset of travelling fronts, the speed is small and we demand that $v = d\xi_0/dt$ be order ε . In order to recover the pitchfork normal form in (17), we set $\tau = \varepsilon^2 t$. Next, recall that the transition to travelling fronts occurs for $\delta = \alpha^2$. Hence we unfold the dynamics nearby by setting $\delta = \alpha^2 + \varepsilon^2 \delta_2$. Third, we fix $(x_t - x + x^3 + y)\rho = O(\varepsilon^3)$, which determines when the effects of discreteness enter the expansion.

We next introduce the asymptotic sequence, $x = x_0 + \varepsilon x_1 + \varepsilon^2 x_2 + \varepsilon^3 x_3$. The subscripts here refer to the asymptotic ordering of the solution, which introduces a notational conflict with the earlier use of the subscript n to mean a lattice point for the discrete system. However, by this point, the discrete spatial coordinate appears as a proper argument of x via the continuous coordinate ξ , and so we continue with this conflict to present the asymptotic theory in a conventional manner; we hope this causes no confusion to the reader. The stage is now set to introduce the asymptotic sequences and scalings into the governing equations, expand, and solve the system order by order in ε .

At leading order, we obtain (15) and the equilibrium front, but with a time-dependent position. We write the solution in the form,

$$x_0(\xi, \tau) = \sqrt{1 - \alpha} \tanh \sqrt{\frac{1 - \alpha}{d}} \left(\xi - \frac{X(\tau)}{\varepsilon} \right), \quad (21)$$

where the front position, $\xi_0 = X(\tau)/\varepsilon$, is written in such a way that the speed, $\varepsilon^2 \dot{\xi}_{0\tau}$, is order ε . That is, $x_{0t} \rightarrow -\varepsilon \dot{X} x_{0\xi}$. This scaling is needed because, in the continuum limit, the width of the front becomes large and the front position must traverse many lattice points to shift the profile. The scaling is also demanded by the pitchfork normal form in (17).

At order ε , we arrive at the equation,

$$Lx_1 \equiv \frac{1}{2}d x_{1\xi\xi} + (1 - \alpha)x_1 - 3x_0^2x_1 = 0, \quad (22)$$

and it is convenient to set $x_1 = 0$. At order ε^2 ,

$$Lx_2 = \frac{1}{\alpha}\dot{X}^2x_{0\xi\xi} \quad \longrightarrow \quad x_2 = \frac{1}{2\alpha}\dot{X}^2\xi x_{0\xi}. \quad (23)$$

Finally, at order ε^3 ,

$$Lx_3 = \frac{\rho}{\varepsilon^3} [x_0^3 - (1 - \alpha)x_0] - \frac{1}{\alpha}\ddot{X}x_{0\xi} + \frac{1}{\alpha^2}\dot{X}^3x_{0\xi\xi\xi} - \frac{\delta_2}{\alpha^2}\dot{X}x_{0\xi}. \quad (24)$$

The operator, L , is self adjoint and has the null vector, $x_{0\xi}$, which is the relic of translational invariance in leading order. Hence, for regularity, the solution must satisfy a solvability condition, obtained on multiplying by the null vector and integrating. This furnishes the relation,

$$\frac{4(1 - \alpha)^{3/2}}{3\alpha d^{1/2}} \left(\ddot{X} + \frac{\delta_2}{\alpha}\dot{X} \right) + \frac{16(1 - \alpha)^{5/2}}{15d^{3/2}}\dot{X}^3 = \frac{d}{2\varepsilon^3} \int_{-\infty}^{\infty} \rho(\xi)x_{0\xi}x_{0\xi\xi}d\xi. \quad (25)$$

We now indulge in a little algebra: We use the Poisson-sum in (20) to write the right-hand side of (25) in the form,

$$\frac{d}{2\varepsilon^3} \sum_{k=1}^{\infty} \int_{-\infty}^{\infty} \cos(2\pi k\xi) (x_{0\xi})_{\xi}^2 d\xi = \frac{4d\pi^3}{3\varepsilon^3} \sum_{k=1}^{\infty} \frac{k^2(1 - \alpha + \pi^2 k^2 d) \sin(2\pi kX/\varepsilon)}{\sinh[\pi^2 k \sqrt{d/(1 - \alpha)}]}. \quad (26)$$

which follows from the integral,

$$\int_{-\infty}^{\infty} \operatorname{sech}^4(q\xi) \cos(2\pi k\xi) d\xi = \frac{4\pi^2 k}{3q^2 \sinh(\pi^2 k/q)} \left(1 + \frac{\pi^2 k^2}{q^2} \right). \quad (27)$$

Equation (26) explicitly writes the effect of discreteness in terms of a rapidly varying factor with the scale of the underlying lattice.

Finally, we are in a position to identify the small parameter ε . As d becomes large, the discreteness term becomes order one because $2 \sinh[\pi^2 k \sqrt{d/(1 - \alpha)}] \sim \exp[\pi^2 k \sqrt{d/(1 - \alpha)}]$ is exponentially large. Thus, we set

$$\varepsilon^3 \sim \exp \left[-\pi^2 \sqrt{d/(1 - \alpha)} \right], \quad (28)$$

which signifies that d need not be especially large, and so we leave algebraic powers of d in the final formulae, and only drop the higher powers of ε . This truncates the sum at $k = 1$ to leave the term,

$$\frac{4\pi^3 d(1 - \alpha + \pi^2 d) \sin(2\pi X/\varepsilon)}{3\varepsilon^3 \sinh \left[\pi^2 \sqrt{d/(1 - \alpha)} \right]}. \quad (29)$$

We now arrive at an amplitude equation, which we quote in terms of the original time variable and front position:

$$\frac{d^2 \xi_0}{dt^2} + \frac{(\delta - \alpha^2)}{\alpha} \frac{d\xi_0}{dt} + \frac{4(1 - \alpha)}{5\alpha d} \left(\frac{d\xi_0}{dt} \right)^3 = \frac{\alpha\pi^3 d^{3/2}(1 - \alpha + \pi^2 d)}{(1 - \alpha)^{3/2} \sinh \left[\pi^2 \sqrt{d/(1 - \alpha)} \right]} \sin 2\pi \xi_0. \quad (30)$$

For the Lorenz case, we may follow the same procedure, expanding about the critical value, $\sigma = \sigma_c$, given by (13). The derivation is more long-winded, but we arrive at an equation with the same form:

$$\ddot{\xi}_0 - \frac{25b^2(3r+2)(\sigma - \sigma_c)\dot{\xi}_0}{3(r-1)(14\sigma_c^2 + 14b^2 + 3b\sigma_c) - 125rb^2} + \Omega\dot{\xi}_0^3 = \frac{250\pi^3\sigma_c^2b^2d^{3/2}(r-1 + \pi^2d)e^{-\pi^2\sqrt{d/(r-1)}}\sin 2\pi\xi_0}{(r-1)^{3/2}[3(r-1)(14\sigma_c^2 + 14b^2 + 3b\sigma_c) - 125rb^2]}, \quad (31)$$

where Ω is a complicated integral that is best evaluated numerically and depends only on r and b . Again the term introducing discreteness is exponentially small in \sqrt{d} .

4.2 The amplitude equation

We quote the amplitude equation in the form,

$$\ddot{\xi}_0 + \Upsilon\dot{\xi}_0 + \Omega\xi_0^3 = \Delta \sin 2\pi\xi_0. \quad (32)$$

This is the equation for a dissipative pendulum, which we now demonstrate provides a compact description of the front transition in a discrete system close to the continuum limit.

The fixed points of (30) lie at $\xi_0 = m$ and $\xi_0 = m + 1/2$, where m is any integer. The former are the centred kinks, the latter are the off-centred ones. For $\Delta > 0$, the centred kinks are always unstable and correspond to saddle points; the off-centred kinks are elliptic fixed points at $\Upsilon = 0$ but become unstable once Υ is decreased through zero. (The stabilities of the two types of kinks are switched if $\Delta < 0$.) Thus, kink stability is correctly recovered in the amplitude equation, since $\Delta > 0$ according to (30) and (31). Also, if $\Delta = 0$, we recover the normal form of the pitchfork bifurcation. The steady continuum front speeds are $\dot{\xi}_0 = 0$ and $\pm\sqrt{-\Upsilon/\Omega}$. The bifurcation is supercritical when $\Omega > 0$, and subcritical if $\Omega < 0$, a feature that is not changed by the discreteness term if $\Delta \neq 0$.

In figure 15 we show phase portraits of the system (32) for different parameter settings. These portraits illustrate how the amplitude equation qualitatively captures aspects of the nonlinear behaviour of the lattice models shown earlier: The top row of pictures show the supercritical situation with $\Omega > 0$. Parameters are selected so that we march through the Hopf and gluing bifurcations on proceeding from left to right, and the phase portraits are qualitatively similar to the reconstructions shown in figure 5. The lower row of panels shows the subcritical case ($\Omega < 0$). Now, the solution diverges once instability sets in, or if the initial condition is placed outside the unstable limit cycle. The amplitude equation does not therefore capture the saddle-node bifurcation and stable travelling kink of the discretized Fitz-Hugh-Nagumo model. The dynamics near the static kink solutions is qualitatively reproduced, however, as can be seen by comparing with the reconstructions of figure 13.

We next briefly discuss the amplitude equation in the instance that the Hopf bifurcation is *supercritical*. *i.e.* $\Omega > 0$. In this case, the change of variables,

$$t = \frac{\hat{t}}{\sqrt{2\pi\Delta}}, \quad \xi_0 = \frac{\phi + \pi}{2\pi}, \quad \alpha = -\frac{2\pi\Upsilon}{\Omega\Delta}, \quad \gamma = \frac{\Omega}{4\pi^2}\sqrt{2\pi\Delta}, \quad (33)$$

places the amplitude equation into a more standard form:

$$\ddot{\phi} + \sin \phi = \gamma\dot{\phi}(\alpha - \dot{\phi}^2). \quad (34)$$

Some results based on this equation are shown in figures 16 and 17. The first picture illustrates the parameter setting for α that gives the heteroclinic connection; the second shows a selection of oscillation periods and average fronts speeds, defined as either $\langle \dot{\phi} \rangle$ or $\sqrt{\langle \dot{\phi}^2 \rangle}$. The structure of the curves in figure 17 resembles the shapes seen in figure 6, modulo the fact that the speeds are plotted using different parameters.

For $\gamma \ll 1$, the method of averaging can be used to find the asymptotic solution,

$$\sin \frac{1}{2}\phi = \text{sn} \left(\frac{t + \Phi}{k}; k \right), \quad (35)$$

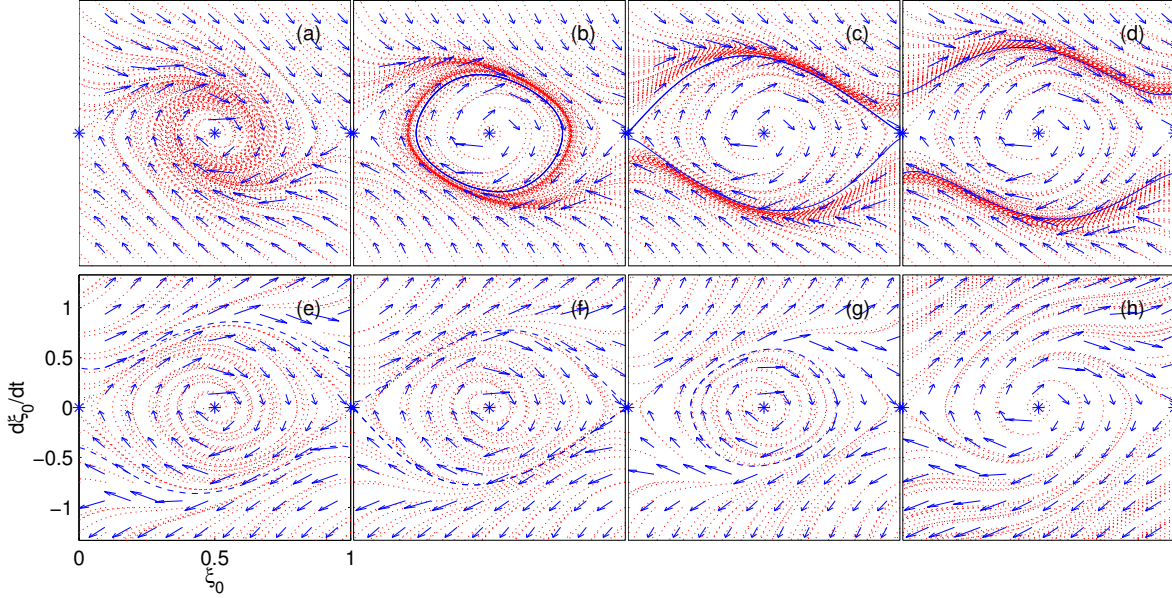


Figure 15: Phase portraits of the model system (32) with $\Delta = 1$. Panels (a)–(d) show the supercritical case ($\Omega > 0$). In panel (a) the central fixed point is stable ($\Upsilon = \Omega = 1$), whereas (b)–(d) show cases with unstable fixed points ($\Upsilon = -1$ and $\Omega = 4, 2.4914$ and 2 , respectively). The solid lines show stable supercritical periodic orbits, the fixed points are marked by stars and sample trajectories by dotted lines. Panels (e)–(h) show the subcritical case ($\Omega < 0$). In panels (e)–(g), the central fixed point is unstable ($\Upsilon = 1$ and $\Omega = -2, -2.4914$ and -4 , respectively), whilst in (h) both fixed points are unstable ($\Upsilon = -1$ and $\Omega = -0.1$). The dashed lines show the unstable periodic orbits.

where $\text{sn}(u; k)$ denotes an elliptic function, Φ is a slowly varying phase and k satisfies the ODE,

$$\dot{k} = \frac{\gamma}{3kK(k)} [(16 - 3\alpha k^2 - 8k^2)E(k) - 4(1 - k^2)K(k)], \quad (36)$$

where $E(k)$ and $K(k)$ are the usual elliptic integrals. This ODE predicts that the system converges to the stable fixed point, $k = k_*$, given by

$$(16 - 3\alpha k_*^2 - 8k_*^2)E(k_*) = 4(1 - k_*^2)K(k_*). \quad (37)$$

If $k_* < 1$, the orbit is “open” and corresponds to a winding solution of the pendulum, or a travelling front. If $k_* > 1$, the stable orbit corresponds to a closed oscillation of the pendulum; a pulsating kink. The separatrix corresponds to $k_* = 1$, giving $\alpha = 8/3$. Once the system has converged to the stable orbit, the period of the orbit is $2kK(k)$ if $k < 1$, or $4kK(k)$ if $k > 1$. Suitable averages then predict the fronts speeds,

$$\langle \dot{\phi} \rangle \equiv \frac{\pi}{kK(k)} \quad \text{and} \quad \sqrt{\langle \dot{\phi}^2 \rangle} \equiv 2\sqrt{\frac{E(k)}{k^2K(k)}}. \quad (38)$$

These small- γ predictions are also drawn in figures 16 and 17 (where they lie on top of the data for $\gamma = 0.025$).

For $\gamma \gg 1$, a regular perturbation expansion predicts that

$$v \equiv \dot{\phi} = \sqrt{\alpha} - \frac{\gamma^{-1}}{2\alpha} \sin \sqrt{\alpha}(t + \Phi) - \frac{\gamma^{-2}}{16\alpha^{5/2}} [5 - \cos 2\sqrt{\alpha}(t + \Phi) - 4\alpha \cos \sqrt{\alpha}(t + \Phi)]. \quad (39)$$

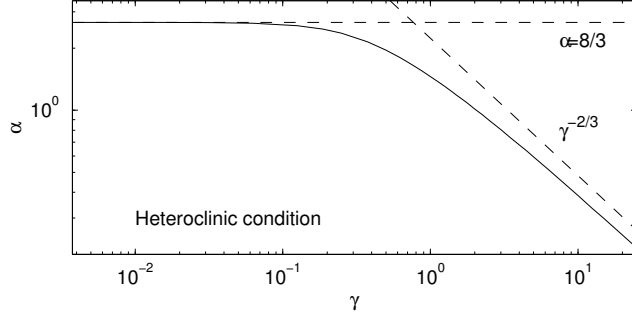


Figure 16: Location of heteroclinic bifurcation for (34) on the (γ, α) -plane. The dashed lines indicate the predictions of asymptotic analysis for small and large γ .

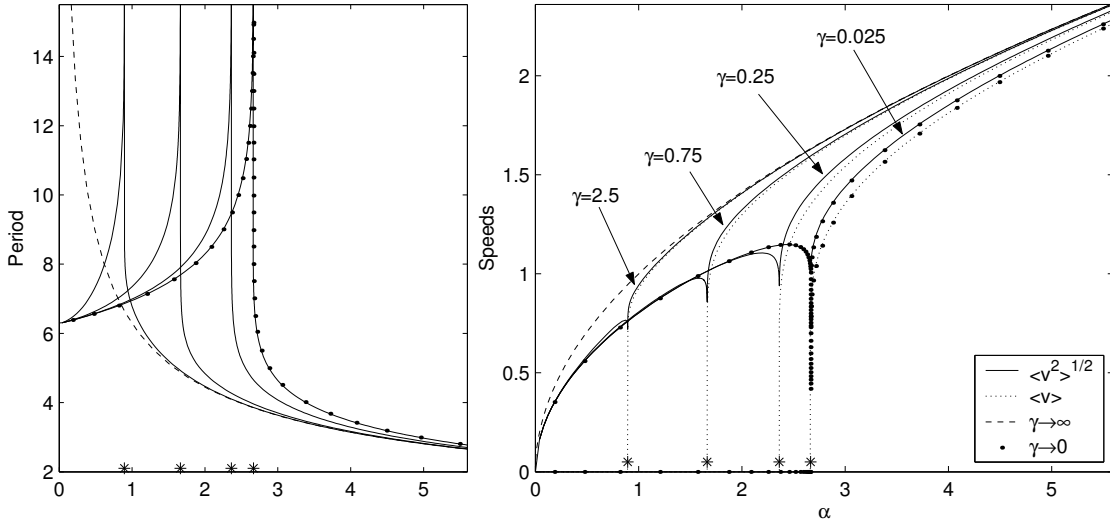


Figure 17: (a) Periods and (b) front speeds against α for four values of γ (as indicated), computed from (34) using the final solution to which the system converges from arbitrary initial conditions. The stars indicate the heteroclinic connection. Also shown are the prediction of asymptotic analysis for small and large γ .

The orbital period is given by $2\pi/\sqrt{\alpha}$, and the average speeds are

$$\langle v \rangle \sim \sqrt{\alpha} - \frac{5\gamma^{-2}}{16\alpha^{5/2}} \quad \text{and} \quad \sqrt{\langle v^2 \rangle} \sim \sqrt{\alpha} - \frac{\gamma^{-2}}{4\alpha^{5/2}}, \quad (40)$$

which suggest that $\alpha \sim \gamma^{-2/3}$ at the heteroclinic point for large γ , as seen in figure 16. In terms of the original parameters, the heteroclinic connection is therefore expected to occur at a value of Υ (*i.e.* $\sigma - \sigma_c$ in Lorenz example or $\delta - \delta_c$ in Fitz-Hugh-Nagumo model) that scales with Δ (*i.e.* $\exp(-\pi^2\sqrt{d/(r-1)})$ or $\exp(-\pi^2\sqrt{d/(1-\alpha)})$) for strong discreteness, or $\Delta^{2/3}$ for weak discreteness.

4.3 Critique

The comparison of the amplitude equation with the original lattice systems is thus far only qualitative. In fact, more quantitative agreement is not possible because of a flaw in the asymptotic derivation. More

specifically, the derivation extracts the leading-order effect of discreteness as an exponentially small correction. This correction is also at the heart of the de-pinning transition in discretized reaction-diffusion equations [3] and the Peierls-Nabarro potential barrier for discrete nonlinear field theories [17]. However, in those contexts it is known that the discreteness correction lies beyond all orders of a traditional asymptotic expansion, and an involved analysis of the complex plane is necessary to derive correctly its detailed form [18]. This difficulty also applies here, and is not surprising in view of the fact that the asymptotic theory attempts to approximate the solution at leading order by a smooth function. Yet it is clear from the reformulation in (18) that the discrete solution has discontinuous derivatives at the lattice points.

To illustrate the point, we consider the oscillation (pulsation) frequency at the Hopf bifurcation, displayed in figures 2 and 8. The amplitude equation predicts this frequency to be $\sqrt{2\pi\Delta}$. But as seen in the figures, whilst the prediction has the correct limiting, exponential dependence on d , it is in error by a factor of order unity. This feature is equivalent to the well-known inability of conventional asymptotics to predict correctly the Peierls-Nabarro frequency [16, 17].

It turns out that it is possible to use a higher-order approximation scheme based on [15] and motivated by the method of averaging, to try to improve this comparison (we do not present the full details for reasons described momentarily): The scheme introduces a change of variables of the form,

$$x(\xi, t) = X(\xi, t) + \frac{2}{d}X_2(\xi, t) + \dots, \quad u(\xi, t) \equiv x_\xi = U(\xi, t) + \sqrt{\frac{2}{d}}U_1(\xi, t) + \frac{2}{d}U_2(\xi, t) + \dots, \quad (41)$$

that builds in part of the non-smooth structure of the discrete solution. In particular, we fix $U_1 = g(\xi)Q(X)$, where $g'(\xi) = \rho(\xi)$ and $Q(X)$ is a suitable chosen function to eliminate the leading-order ‘‘rapidly varying’’ terms proportional to $\rho(\xi)$ in (18). This procedure explicitly places jumps into the derivative of x , and simultaneously smooths (by an integration) the discreteness terms and pushes them to higher order in $\sqrt{2/d}$. The scheme can be iterated to improve further the accuracy. By appropriately working this scheme into the asymptotic expansion, we arrive at a sequence of approximations that lead to the amplitude equation,

$$\ddot{\xi}_0 + \Upsilon\dot{\xi}_0 + \Omega\xi_0^3 = \Delta \sin 2\pi\xi_0, \quad (42)$$

where the left-hand side is the part expected from the continuum model. The right-hand side is similar to that derived earlier, although the coefficient, Δ , now depends on the iteration order of the ‘‘averaging’’ scheme: for the Fitz-Hugh-Nagumo model, and to leading order in d^{-1} ,

$$\begin{aligned} \text{First - order : } & \Delta = \Delta_0 \\ \text{Second - order : } & \Delta = \Delta_0[1 + (\pi^2 - 3)/60] \\ \text{Third - order : } & \Delta = \Delta_0[1 + (\pi^2 - 3)/60 + 3/280], \end{aligned} \quad (43)$$

where

$$\Delta_0 = \frac{\alpha\pi^5 d^{5/2}}{(1 - \alpha)^{3/2} \sinh \pi^2 \sqrt{d/(1 - \alpha)}}, \quad (44)$$

is equivalent to the coefficient found earlier. Each iteration therefore creates a term of the same exponential form, but with an increasingly small algebraic factor. This reflects the attempt of the theory to approximate a term that lies beyond all orders and generates a series for the actual numerical prefactor; ‘‘exponential asymptotics’’ presumably sums that series [18]. Notably, the theory never corrects either the position of the Hopf bifurcation (Υ), nor the cubic nonlinearity (Ω).

Surprisingly, figures 2 and 8 also reveal more serious problems with the amplitude equation than simply an incorrect prefactor in Δ : The numerical data clearly shows that the stability boundaries ($\sigma = \sigma_c$ and $\delta = \delta_c$, or $\Upsilon = 0$) are significantly shifted by discreteness. The position of the heteroclinic connection in the Lorenz case also disagrees with the predictions of the amplitude equation ($\sigma - \sigma_c$ should scale more strongly with d than is the case in figure 2). Worse still, the amplitude equation predicts that the Hopf bifurcation for the Fitz-Hugh-Nagumo example should be *supercritical*, yet numerical computations show that it is, in fact,

subcritical. In other words, not only is the coefficient of the discreteness term in the amplitude equation in error by a factor of order unity, but the other coefficients are also apparently incorrect, and can even have the wrong sign. This problem signifies that there are deep difficulties in extracting the correct coefficients by the asymptotics used above.

5 Discussion

We summarize the main conclusion as follows: At the continuum front bifurcation where moving fronts are created, there is a multiple, zero eigenvalue. Adding discreteness lifts this degeneracy similarly to how it destroys the translational zero eigenvalue. For the centred kinks, the eigenvalue pair splits on the real axis, leading to two real eigenmodes of which one is unstable. For off-centred kinks, the pair splits on the imaginary axis leading to a complex pair which become unstable in a Hopf bifurcation. Moreover, in the continuum limit, the centred kink is located very close in phase space. Thus the limit cycles shed at the Hopf bifurcation quickly collide with the centred kink in a gluing, heteroclinic bifurcation, which leaves a travelling front. In cases where the Hopf bifurcation is supercritical, stable pulsating kinks mediate the transition from static to moving fronts. If the Hopf is subcritical, on the other hand, there is an immediate transition to a stable travelling kink which is born in a third saddle-node bifurcation at smaller coupling strengths (this subcritical scenario also appears to characterize the discretized version of the complex Ginzburg-Landau equation of [6]). In other words, the simple pitchfork of the continuum transition is replaced by a sequence of at least two different bifurcations in the discretized model.

By performing a perturbation analysis in the continuum limit, we have presented an equation that qualitatively captures the low-amplitude behaviour of the discrete system. Unfortunately, the coefficients of the model are quantitatively in error apparently as a result of the beyond-all-orders nature of the effect of discreteness; our derivation provides the correct scaling of discrete effects, but not their detailed expression. We leave this issue as an open mathematical problem.

Nevertheless, the model proves useful in discussing other aspects of the problem. For example, in the continuum problem it is known that the pitchfork becomes an imperfect bifurcation when the left-right symmetry of propagation is broken [5]. Figure 18 shows the bifurcation diagram that results when we discretize the imperfect problem. The diagram is obtained by solving the modified amplitude equation,

$$\ddot{\phi} + \sin \phi = \gamma \dot{\phi}(\alpha - \dot{\phi}^2) + \mu, \quad (45)$$

where μ is a parameter determining the degree of symmetry breaking; the new term in (45) appears in the asymptotic theory on adding, for example, a small constant to the y -equation of the Fitz-Hugh-Nagumo model which breaks symmetry in that original system (*cf.* [5]). Figure 18 illustrates how the more slowly moving fronts become pinned when the system is made discrete, and pulsating kinks again appear in a Hopf bifurcation. However, the full story is complicated significantly by the combined effects of the breakage of symmetry and discreteness.

In this article, we have considered systems for which some degree of analysis is possible, but we have resorted to numerical techniques to shore up the theory. A greater degree of analysis is often afforded in models in which the nonlinearities of the governing equations are replaced by piece-wise linear functions. This leads to analytical simplifications, such as the construction of explicit travelling front solutions for both continuum systems (*e.g.* [15]) and discrete lattices [19, 20]. In the Appendix, we consider two models of this kind to explore whether we may make further analytical headway in quantifying the front bifurcation. As it turns out, these piece-wise linear models have quite different bifurcation properties, which cautions against blindly replacing smooth nonlinearity with a piece-wise linear function.

Finally, we should remark that the discretizations of the PDEs we have considered are equivalent to a nearest-neighbour coupling scheme. Yet it is known that such a discretization can lead to undesired behaviour when used as a numerical scheme. Indeed, several of our results could be viewed as building on that idea. However, other discretizations are possible, and the ramifications on the front transition may well be different.

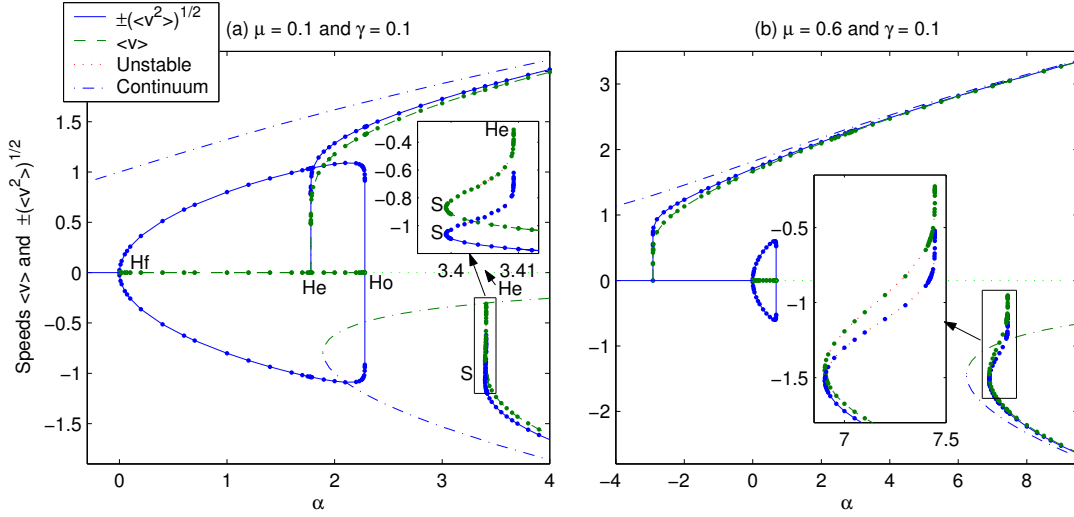


Figure 18: Front speeds predicted by equation (45). Shown are the average speeds defined in (4) against α for $\gamma = 0.1$ with (a) $\mu = 0.1$ and (b) $\mu = 0.6$. The figure also shows when Hopf (Hf), saddle-node (S), heteroclinic (He), and homoclinic (Ho) bifurcations occur. The dashed-dotted lines indicate the imperfect bifurcation expected for the continuum case. Unlike in figure 17, we now show the positive and negative branches of the front speed, which are no longer the same on reflection.

Acknowledgements: This work was performed whilst two of the authors (NJB and AK) were visiting the Mathematics Department at M.I.T., which we thank for hospitality. AK thanks the Development and Promotions of Science and Technology Talents Project of the Thai government for support.

A Piece-wise linear models

In this appendix, we consider two models that admit more analysis than the systems explored in the main text. These are models generated by replacing the smooth, cubic nonlinearity of the Fitz-Hugh-Nagumo model by piece-wise linear functions. More specifically, we consider the models,

$$\dot{x}_n = F(x_n) - (y_n - \alpha x_n) + \frac{d}{2}(x_{n+1} + x_{n-1} - 2x_n), \quad \dot{y}_n = \delta \left(x_n - \frac{1}{\alpha} y_n \right) + \frac{\beta d}{2}(y_{n+1} + y_{n-1} - 2y_n), \quad (46)$$

with the choices

$$F(x_n) = \begin{cases} -\sqrt{1-\alpha} - x_n, & x_n < -\sqrt{1-\alpha}/2 \\ x_n, & -\sqrt{1-\alpha}/2 \leq x_n \leq \sqrt{1-\alpha}/2 \\ \sqrt{1-\alpha} - x_n, & \sqrt{1-\alpha}/2 < x_n \end{cases} \quad (47)$$

or

$$F(x_n) = \begin{cases} -\sqrt{1-\alpha} - x_n, & x_n < 0 \\ 0, & x_n = 0 \\ \sqrt{1-\alpha} - x_n, & 0 < x_n \end{cases} . \quad (48)$$

The first of these piecewise linear solutions is continuous, whereas the second is discontinuous. We have also added a second diffusive/coupling term to the y -equation, with a coupling strength that is different from that appearing in the x -equation (and given by the parameter β). For the continuum limit of these models, we replace $x_{n+1} + x_{n-1} - 2x_n$ and $y_{n+1} + y_{n-1} - 2y_n$ by the spatial derivatives, $\partial^2 x / \partial \xi^2$ and $\partial^2 y / \partial \xi^2$, respectively.

A.1 The case (47), with $\beta = 0$

For the continuum version of the problem, the static front may be built in terms of exponential functions. Linear stability theory then indicates that the eigenvalues (growth rates), λ , satisfy the dispersion relation,

$$\sqrt{1 - \Lambda} = \sqrt{1 + \Lambda} \tan\left(\frac{\pi}{4}\sqrt{1 - \Lambda}\right), \quad \Lambda = \lambda - \frac{\alpha^2 \lambda}{\delta + \alpha \lambda}. \quad (49)$$

The relevant solution is $\Lambda = 0$, which gives

$$\lambda(\alpha \lambda - \alpha^2 + \delta) = 0, \quad (50)$$

and reveals the mode reflecting translational invariance together with another localized mode that becomes unstable for $\delta < \alpha^2$.

In the discrete version of the model, the key parameter turns out to be the number of lattice sites, M , that are contained in the “core” of the kink (*i.e.* the number of sites with $|x_n| < \sqrt{1 - \alpha/2}$), which in turn depends on d . This quantity is plotted in figure 19 for both centred and off-centred kinks. As d increases, M jumps discontinuously by 2 as lattice sites move symmetrically into the core. For large d , $M \sim (\pi/2)\sqrt{d/2}$, which can be established analytically.

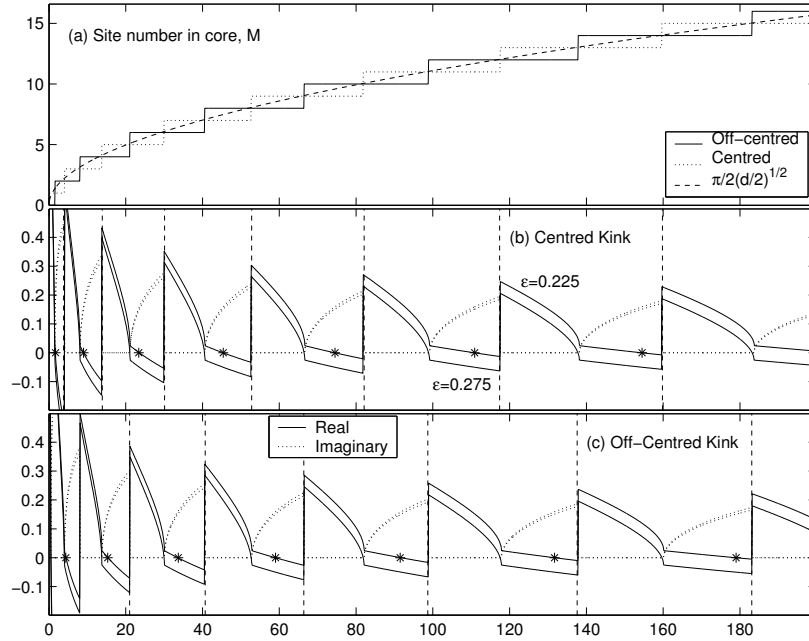


Figure 19: (a) The number of lattice sites, M , within the core of the centered and off-centered, static kinks against d . Panels (b) and (c) show the corresponding eigenvalues of the most unstable modes for $\delta = 0.225$ and 0.275 . In the former case, the stars show the Hopf bifurcations. $\alpha = 1/2$.

The dispersion relation for the eigenmodes of the discrete kinks is

$$1 - RS + R^M(R - S) = 0, \quad (51)$$

where

$$R = 1 + (\Lambda - 1)/d + i\sqrt{1 - [1 + (\Lambda - 1)/d]^2}, \quad S = 1 + (\Lambda + 1)/d - \sqrt{[1 + (\Lambda + 1)/d]^2 - 1}$$

and Λ is again given by (49). Only through M does the equilibrium kink profile appear in the stability theory. The relevant solution for Λ is real and satisfies $S \cos(M-1)\theta/2 = \cos(M+1)\theta/2$, where $\cos \theta = 1 + (\Lambda - 1)/d$, which then predicts

$$\lambda = \frac{1}{2} \left(\alpha + \Lambda - \frac{\delta}{\alpha} \right) \pm \sqrt{\frac{1}{4} \left(\alpha + \Lambda - \frac{\delta}{\alpha} \right)^2 + \frac{\delta \Lambda}{\alpha}}. \quad (52)$$

Eigenvalues of the most unstable modes for the centred and off-centred kinks are illustrated in figure 19. As lattice sites move into the core of the kink, the eigenvalues vary abruptly and the stability changes discontinuously. The stability of the two kink types is closely connected, creating a continual switching of kink stability. For $\delta > \alpha^2$, where one kink becomes unstable, the other is stabilized. For $\delta < \alpha^2$, there is a additional sequence of destabilizing Hopf bifurcations as d is varied. The complicated array of bifurcations revealed in figure 19 is far richer than in the model of the main text with smooth nonlinearity. One common feature, however, is that the Hopf bifurcations appear to be invariably subcritical, and the unstable pulsating kink solutions undergo heteroclinic connections to create unstable travelling kinks which turn around in nearby saddle-node bifurcations to furnish stable travelling fronts (at least in the numerical computations we have conducted).

In the continuum limit, $M \sim (\pi/2)\sqrt{d/2}$ and (51) can be reduced to the continuum relation (49) to leading order. However, because M must be an integer, Λ no longer vanishes exactly, and one can show that $\Lambda \rightarrow (2M/\pi)\sqrt{2/d} - 1 \sim O(d^{-1/2})$. Thus,

$$\lambda \left(\lambda + \frac{\delta}{\alpha} - \alpha \right) \sim O(d^{-1/2}). \quad (53)$$

In other words, the small correction due to discreteness is algebraically small in d^{-1} . By contrast, in the model of the main text with smooth nonlinearity the discreteness term is exponentially small (*cf.* [15]).

A.2 The case (48)

For the second example, a first problem that we encounter is that $F(x_n)$ is discontinuous at the origin. Only by fixing $F(0) = 0$ as the value at the discontinuity, can the discrete model support centred kinks. However, these structures are pathological creatures because they must be positioned exactly at the discontinuity; any solution falling arbitrarily close to this kink moves steadily away from it as though that equilibrium solution did not exist (which is the analogue of the exponential instability of the centred kink in the continuous models). As a result, the solution cannot participate in the bifurcation creating travelling fronts, which consequently proceeds down a different pathway in this model.

An exercise in algebra establishes that the continuum model corresponding to (46) and (48) has the static kink solution $x(\xi, t) = X(\xi)$, with

$$X = \sqrt{1 - \alpha} \left[1 + \frac{(m_2^2 - 1)e^{-m_1|\xi|} + (m_1^2 - 1)e^{-m_2|\xi|}}{m_1^2 - m_2^2} \right], \quad (54)$$

where m_1 and m_2 are the two solutions to the quartic equation, $\beta m^4 + m^2(\alpha\beta - \beta - \delta/\alpha) + \delta/\alpha = 0$, with positive real part. Linear perturbations to this kink with the normal-mode form, $(\hat{x}, \hat{y})e^{\lambda t}$, satisfy

$$\left(\lambda + 1 - \alpha - \frac{\partial^2}{\partial \xi^2} \right) \hat{x} + \hat{y} = 2\sqrt{1 - \alpha} \hat{x}(0) \delta[X(\xi)] \equiv 2\sqrt{1 - \alpha} \frac{\hat{x}(0)}{X'(0)} \delta(\xi), \quad (55)$$

and

$$\left(\lambda + \frac{\delta}{\alpha} - \beta \frac{\partial^2}{\partial \xi^2} \right) \hat{y} - \delta \hat{x} = 0, \quad (56)$$

where the delta-function appears by virtue of the perturbation of the discontinuity in $F(x)$ (and the motion of the kink's centre). The dispersion relation can then be derived:

$$\frac{m_1 + m_2}{m_1 m_2} = \frac{M_1 M_2}{M_1 M_2 + m_1^2 m_2^2 + \lambda/\beta}, \quad (57)$$

where M_1 and M_2 are the two solutions to

$$\beta M^4 + M^2(\alpha\beta - \beta - \delta/\alpha - \lambda - \beta\lambda) + \lambda^2 + \lambda(1 - \alpha + \delta/\alpha) + \delta/\alpha = 0,$$

with positive real part. Travelling fronts appear at the critical value of δ given by the equation,

$$\left(\frac{\delta}{\alpha\beta} + 1 - \alpha + 2\sqrt{\frac{\delta}{\alpha\beta}}\right) \left(\frac{\delta}{\alpha} + 1 - \alpha - 2\beta\right) + \left(1 + \sqrt{\frac{\delta}{\alpha\beta}}\right) \left[\frac{\delta}{\alpha} + 1 - \alpha + (1 + \beta)\sqrt{\frac{\delta}{\alpha\beta}}\right] = 0. \quad (58)$$

For $\beta = 1$, the critical condition is expressed much more simply as $\delta = \alpha(1 + 2\alpha - \sqrt{1 + 4\alpha})/2$. The wavespeed of the moving front away from the bifurcation point can further be constructed algebraically (some results are shown in figure 20).

The off-centred discrete kinks have lattice sites that are placed a finite distance from the discontinuity in $F(x)$. As a result, the normal modes, with amplitudes, $(\hat{x}_n, \hat{y}_n)e^{\lambda t}$, satisfy the difference equations,

$$(\lambda + 1 - \alpha)\hat{x}_n - \frac{d}{2}(\hat{x}_{n+1} + \hat{x}_{n-1} - 2\hat{x}_n) - \hat{y}_n = 0, \quad \left(\lambda + \frac{\delta}{\alpha}\right)\hat{y}_n - \frac{\beta d}{2}(\hat{y}_{n+1} + \hat{y}_{n-1} - 2\hat{y}_n) - \delta\hat{x}_n = 0, \quad (59)$$

in which no information regarding the equilibrium kink profile appears. It is readily verified that there are no solutions to these difference equations that decay both to the left and right of the kink. In other words, the kinks support only a pure continuous eigenspectrum and there can be no unstable localized modes.

A key difference between the continuum equations in (55)-(56) and the discrete one in (59), is the forcing term on the right of (55) that describes the motion of the kink's core. The addition of only infinitesimal perturbations to the discrete off-centred kink permits no lattice sites to be displaced across the discontinuity to create an analogous source in (59), which is why that kink turns out to be stable. Nevertheless, we may allow perturbations of finite amplitude, and consider displacements that shift one of the nearest lattice sites across the kink centre, to simulate kink motion. The resulting nonlinear stability theory contains an additional source term, $2\sqrt{1 - \alpha}$, in the first equation in (59) at that special lattice site, modelling a shift in the kink position. The problem now admits normal-mode-like solutions. Because such shifts become easier as d increases (and the lattice points cluster closer to the kink core), it is this latter theory which must connect to the stability analysis of the continuum kink in the limit $d \rightarrow \infty$.

Rather than basing an analysis of the discrete model on linear stability theory, we instead turn to a direct computation of the moving fronts in this model, which is possible by virtue of the discontinuous form of $F(x)$. By using Fourier transform methods [19, 20, 21], we reduce the construction of these states to quadrature:

$$X(n - ct) = \frac{2c}{\pi} \int_0^\infty \frac{B \cos k(n - ct)}{A^2 + c^2 k^2 B^2} dk - \frac{2}{\pi} \int_0^\infty \frac{A \sin k(n - ct)}{k(A^2 + c^2 k^2 B^2)} dk, \quad (60)$$

where

$$A(k) = d(\cos k - 1) - 1 + \alpha + \delta\alpha \frac{\alpha\beta d(\cos k - 1) - \delta}{[\alpha\beta d(\cos k - 1) - \delta]^2 + \alpha^2 c^2 k^2} \quad (61)$$

and

$$B(k) = 1 - \frac{\delta\alpha^2}{[\alpha\beta d(\cos k - 1) - \delta]^2 + \alpha^2 c^2 k^2}, \quad (62)$$

and the kink speed c is given implicitly by the relation,

$$\frac{2c}{\pi} \int_0^\infty \frac{B dk}{A^2 + c^2 k^2 B^2} = 0. \quad (63)$$

(Note that we have taken the kink centre to lie at $n - ct = 0$, and that the stationary kink with $c = 0$ is always a possible solution.)

A comparison of the kink speeds in the discrete and continuum models is shown in figure 20. This displays how the pitchfork bifurcation that creates two travelling fronts in the continuum model disappears completely in the discrete case. Instead, a new, unstable travelling kink appears at small wavespeed that collides with the stable discrete kink in a saddle-node bifurcation near the original pitchfork. Thus the bifurcation scenario changes dramatically as a result of the discontinuous piece-wise linear function $f(x)$. More details of the solutions are shown in figure 21.

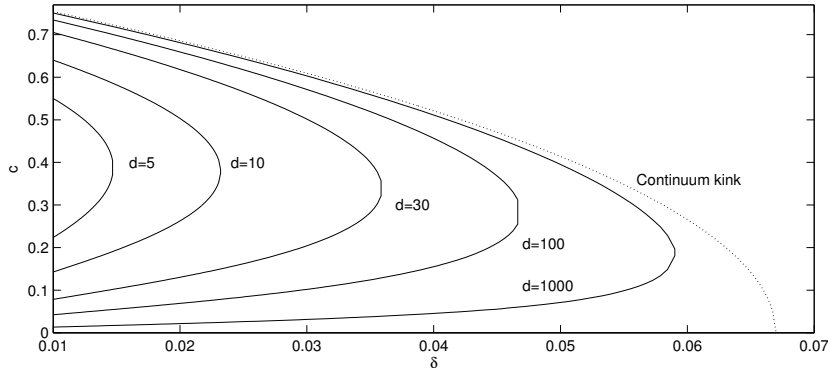


Figure 20: Scaled front speeds, $v = c\sqrt{2/d}$, against δ for the discrete and continuum models with (48). Five curves are shown for different values of d . $\alpha = 1/2$ and $\beta = 1$.

References

- [1] M. Peyrard and M. D. Kruskal, “Kink dynamics in the highly discrete sine-gordon system,” *Physica D* **14**, 88 (1984).
- [2] P. G. Kevrekidis and M. I. Weinstein, “Dynamics of lattice kinks,” *Physica D* **142**, 113 (2000).
- [3] J. P. Keener, “Propagation and its failure in coupled systems of discrete excitable cells,” *Physica D* **47**, 556 (1987).
- [4] D. Pazo and V. Perez-Munuzuri, “Traveling fronts in an array of coupled symmetric bistable units,” *Chaos* **13**, 812 (2003).
- [5] A. Hagberg and E. Meron, “Pattern formation in non-gradient reaction-diffusion systems: the effects of front bifurcations,” *Nonlinearity* **7**, 805 (1994).
- [6] P. Coulet, J. Lega, B. Houchmanzadeh, and J. Lajzerowicz, “Breaking chirality in nonequilibrium systems,” *Phys. Rev. Lett.* **65**, 1352 (1990).
- [7] M. Mimura and M. Nagayama, “Nonannihilation dynamics in an exothermic reaction-diffusion system with mono-stable excitability,” *Chaos* **7**, 817 (1997).
- [8] C. B. Muratov and V. V. Osipov, “Travelling spike autosolitons in the gray-scott model,” *Physica D* **155**, 112 (2001).
- [9] N. J. Balmforth, R. V. Craster, and P. Kevrekidis, “Being stable and discrete,” *Physica D* **135**, 212 (2000).

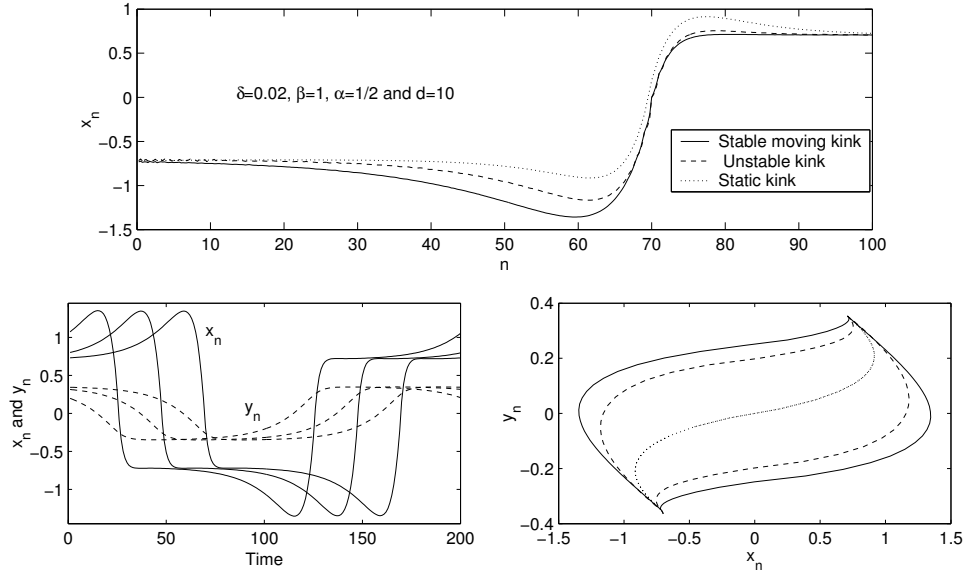


Figure 21: Travelling kink profiles for $\delta = 0.02$, $d = 10$, $\alpha = 1/2$ and $\beta = 1$. The top and final panels show the kink profiles on the moving lattice and as projections onto the (x_n, y_n) -plane (the two reflectionally symmetrical kinks are shown which both propagate forwards). The static kink is also displayed. The second panel shows a realization of the pair of stable, moving kinks in an initial-value problem on a periodic lattice (three snapshots of x_n and y_n are shown, spaced 10 time units apart).

- [10] D. Pazo, N. Montejo, and V. Perez-Munuzuri, “Wave fronts and spatiotemporal chaos in an array of coupled lorenz oscillators,” *Phys. Rev. E* **63**, 066206 (2001).
- [11] D. Pazo and V. Perez-Munuzuri, “Onset of wave fronts in a discrete bistable medium,” *Phys. Rev. E* **64**, 065203(R) (2001).
- [12] N. J. Balmforth, C. Pasquero, and A. Provenzale, “The lorenz-fermi-pasta-ulam experiment,” *Physica D* **138**, 1 (2000).
- [13] K. Josic and C. E. Wayne, “Dynamics of a ring of diffusively coupled lorenz oscillators,” *J. Stat. Phys.* **98**, 1 (2000).
- [14] D. Michaelis, U. Peschel, F. Lederer, D. V. Skryabin, and W. J. Firth, “Universal criterion and amplitude equation for a nonequilibrium ising-bloch transition,” *Phys. Rev. E* **63**, 066602 (2001).
- [15] J. P. Keener, “Homogenization and propagation in the bistable equation,” *Physica D* **136**, 1 (2000).
- [16] S. Flach and K. Kladko, “Perturbation analysis of weakly discrete kinks,” *Phys. Rev. E* **54**, 2912 (1996).
- [17] P. G. Kevrekidis, C. K. R. T. Jones, and T. Kapitula, “Exponentially small splitting of heteroclinic orbits: from the rapidly forced pendulum to discrete solitons,” *Phys. Lett. A* **269**, 120 (2000).
- [18] J. R. King and S. J. Chapman, “Asymptotics beyond all orders and stokes lines in nonlinear differential-delay equations,” *Europ. J. Appl. Math.* **12**, 433 (2001).
- [19] G. Fath, “Propagation failure of travelling waves in a discrete bistable medium,” *Physica D* **116**, 176 (1998).

- [20] C. E. Elmer and E. S. V. Vleck, "Analysis and computation of traveling wave solutions of bistable differential-difference equations," *Nonlinearity* **12**, 771 (1999).
- [21] A. Carpio and L. L. Bonilla, "Oscillatory wave fronts in chains of coupled nonlinear oscillators," *Phys. Rev. E* **67**, 056621 (2003).